Demonstration of a Single-Photon Router in the Microwave Regime

Io-Chun Hoi,[1] C. M. Wilson,[1] Göran Johansson,[1] Tauno Palomaki,[1] Borja Peropadre,[2] and Per Delsing[1]

[1]*MC2, Chalmers University of Technology, Göteborg, Sweden*

[2]*Instituto de Física Fundamental Serrano, CSIC, Madrid, Spain*

(Received 21 February 2011; revised manuscript received 4 June 2011; published 9 August 2011)

We have embedded an artificial atom, a superconducting transmon qubit, in an open transmission line and investigated the strong scattering of incident microwave photons (~ 6 GHz). When an input coherent state, with an average photon number $N \ll 1$ is on resonance with the artificial atom, we observe extinction of up to 99.6% in the forward propagating field. We use two-tone spectroscopy to study scattering from excited states and we observe electromagnetically induced transparency (EIT). We then use EIT to make a single-photon router, where we can control to what output port an incoming signal is delivered. The maximum on-off ratio is around 99% with a rise and fall time on the order of nanoseconds, consistent with theoretical expectations. The router can easily be extended to have multiple output ports and it can be viewed as a rudimentary quantum node, an important step towards building quantum information networks.

DOI: 10.1103/PhysRevLett.107.073601 PACS numbers: 42.50.Gy, 03.67.Hk, 85.25.Cp

In recent years, quantum information science has advanced rapidly, both at the level of fundamental research and technological development. For instance, quantum cryptography systems have become commercially available [1]. These systems are examples of quantum channels, serving mainly to distribute quantum information. There is a significant effort to combine these quantum channels with quantum nodes that would offer basic processing and routing capability. The combination of these channels and nodes would create a quantum network enabling applications simply impossible today [2]. Quantum networks connecting simple quantum processing nodes are also a promising architecture for a scalable quantum computer.

In this Letter, we demonstrate an example of a rudimentary quantum node, a single-photon router. The active element of the router is a single ''artificial atom'', a superconducting qubit, strongly coupled to a superconducting transmission line. Exploiting the phenomenon of electromagnetically induced transparency (EIT), we show that we can route a single-photon signal from an input port to either of two output ports with an on-off ratio of 99%. The switching time of the device is shown to be a few nanoseconds, consistent with theoretical expectations and the device parameters. The device is a nanofabricated circuit offering a clear path to scalability. For instance, it is straight forward to extend this router to select between multiple output channels.

An obvious requirement of a quantum channel is the ability to coherently distribute quantum information over relatively large distances. This typically implies the use of photons as information carriers, as opposed to other quantum systems such as atoms. This presents a problem when trying to implement a quantum node, as the interaction of photons with themselves is vanishingly small. Without interactions, photons cannot be controlled or directed. We can however look to control the photons by using matter as an intermediary [3–5], exploiting the strong interactions of electrons for instance. Still, the coupling of single-photon signals to bulk nonlinear materials is too weak for efficient control. A number of authors [6–9] have suggested that this problem could be overcome by resonantly coupling the signals to single atoms, which are highly nonlinear systems. While impressive technical achievements have been demonstrated in experiment, the coupling of single atoms to light remains relatively inefficient. For instance, in the prototypical experiment of scattering light from a single atom, the reduction in the intensity (extinction) of the incident light does not exceed 12% [10–13]. However, it was recently demonstrated that microwave photons can be coupled extremely efficiently to a single artificial atom, showing extinction efficiencies in an open transmission line greater than 90% [14,15]. Here we demonstrate an extinction of 99.6%, an order of magnitude increase, and use this approach as the basis of our single-photon router.

Our artificial atom is a superconducting transmon [16] qubit, consisting of two Josephson junctions in a SQUID configuration with a total capacitance C_Σ. It is capacitively coupled to a 1D transmission line [see Fig. 1(a)] in a coplanar waveguide configuration. The two lowest energy states $|0\rangle$, $|1\rangle$ have a transition energy $\hbar\omega_{01}(\Phi) \approx \sqrt{8E_J E_c} - E_c \sim 7.1$ GHz where E_J is the Josephson energy of the SQUID, E_C is the charging energy and Φ is the external magnetic flux. This type of qubit has been extensively studied [17–20] and successfully used to, for example, perform quantum algorithms [21] as well as produce single photons [22].

The electromagnetic field in the transmission line can be described by incoming $(+)$ and outgoing $(-)$ voltage waves on the left (L) and the right (R), $V^{\pm}_{L,R}$. In Fig. 1(a), the transmission coefficient $t = V^-_R/V^+_L$ and the reflection coefficient $r = V^-_L/V^+_L$ are related by the definition,

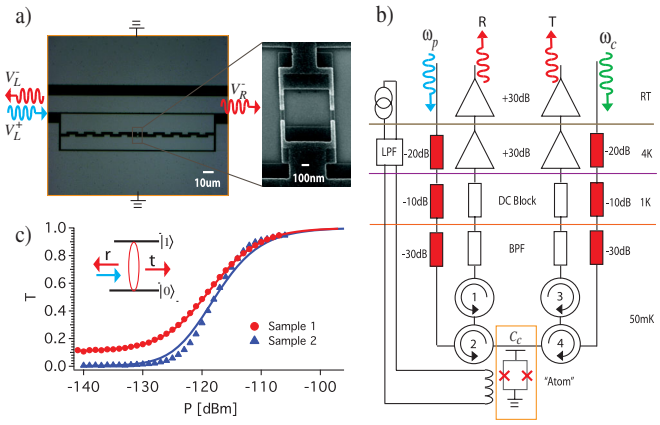

FIG. 1 (color online). Scattering from a single artificial atom. (a) A micrograph of our artificial atom, a superconducting transmon qubit embedded in a 1D open transmission line. The light regions are Al while the dark regions are the oxidized silicon substrate. We see the center conductor of the CPW in between the two ground planes and the two plates of the interdigitated capacitance of the transmon. The enlargement is a scanning-electron micrograph of the SQUID loop of the transmon, which allows us to tune its transition frequency with an external magnetic flux Φ. The junctions are formed using the standard double-angle evaporation technique. (b) Schematic of the measurement setup. A strong control pulse at $\omega_c = \omega_{12}$ is used to route a weak microwave signal at the probe frequency ω_{01}. We measure the transmitted and reflected probe simultaneously in the time domain. The circulators, numbered 1–4, allow us to separate signals propagating in different directions in the lines. (c) Transmittance, $T = |t|^2$, on resonance as a function of incident power. For $N \ll 1$ we see extinction of the coherent probe of 90% and 99.6% for sample 1 and 2, respectively. $N = 1$ for a power of -125 dBm (-123 dBm) for sample 1 (2). The symbols are data while the lines are fits based on Eq. (1). (Inset) A weak, resonant coherent state is scattered by the atom.

$t = r + 1$. When the applied probe frequency ω_p is equal to ω_{01}, the reflection coefficient is given by [14]

$$r = -r_0 \frac{1}{1 + \Omega_p^2/\Gamma_{10}\gamma_{10}}, \tag{1}$$

where the maximum reflection amplitude is $r_0 = 1/(1 + 2\Gamma_\phi/\Gamma_{10})$. Γ_{10} is the relaxation rate of the atom from $|1\rangle$ to $|0\rangle$, $\gamma_{10} = \Gamma_{10}/2 + \Gamma_\phi$ is the 0–1 decoherence rate, and Γ_ϕ is the 0–1 pure dephasing rate. A coherent input signal (probe) will drive coherent oscillations of the atom at a Rabi frequency which is linear in the probe amplitude and can be written as [16]

$$\Omega_p = \frac{2e}{\hbar}\frac{C_c}{C_\Sigma}\left(\frac{E_J}{8E_c}\right)^{1/4}\sqrt{PZ_0}, \tag{2}$$

where $P = |V_L^+|^2/2Z_0$ is the probe power, $Z_0 \sim 50\ \Omega$ is the impedance of the transmission line and C_c is the coupling capacitance between the qubit and the transmission line [Fig. 1(b)]. For a weak resonant probe ($\Omega_p \ll \Gamma_{10}, \gamma_{10}$) and in the absence of both pure dephasing ($\Gamma_\phi = 0$) and unknown loss channels, such as relaxation of the qubit not associated with the coupling to the transmission line, we expect to see full reflection of the incoming probe [7,8,23]. This perfect reflection can be understood as the coherent interference between the incoming wave and the wave scattered from the atom.

TABLE I. Parameters for samples 1 and 2. All values in GHz (except for the extinction), with an uncertainty of 5%.

Sample	E_J/h	E_c/h	$\Gamma_{10}/2\pi$	$\Gamma_\phi/2\pi$	Ext.
1	12.7	0.59	0.073	0.018	90%
2	21.5	0.35	0.096	0.002	99.6%

We have measured the reflection and transmission coefficients in two different samples as a function of incident probe power using homodyne detection (See Supplemental Material [24]). By fitting the frequency and power dependence of this data, we extract the parameters shown in Table I.

In Fig. 1(c), we plot the transmittance $T = |t|^2$ on resonance as a function of P. We can define an average number of photons per interaction time $2\pi/\Gamma_{10}$ as $N \equiv 2\pi P/(\hbar\omega_p\Gamma_{10})$. For $N \ll 1$, we see an extinction of propagating photons of up to 90% for sample 1 and 99.6% for sample 2. The strong saturation of the extinction already at single-photon powers is an indication that the scattering is caused by a single atom, since the atom can only absorb and emit one photon at a time. The reflected power (not shown) also varies with power as expected.

So far, we have considered only the lowest two energy levels of our artificial atom. In reality, the transmon has several higher states, in particular, it has a second excited state with the 1–2 transition frequency ω_{12}. This second transition can be directly measured using two-tone spectroscopy, as is illustrated in Fig. 2(a) for sample 1. We extract $\omega_{12}/2\pi = 6.38$ GHz, giving an anharmonicity of $\alpha = 720$ MHz between the two transitions. The linewidth of the 1–2 transition is dominated by the charge dispersion of $|2\rangle$. Further increasing the pump power, we observe the well-known Mollow triplet [14,25,26] (not shown). The Rabi splitting of the triplet was used to calibrate the applied microwave power at the atom.

By pumping the system at $\omega_c = \omega_{12}$, we can observe the phenomenon of electromagnetically induced transparency (EIT)[15,27–29] based on the Autler-Townes splitting [30,31]. With the pump off, we have seen that an incident, low-power probe at ω_{01} is reflected. For large control powers, however, the original line splits into a doublet with a separation of Ω_c [see Fig. 2(b)], and the atom becomes transparent to the probe beam at ω_{01}.

We exploit EIT to create a single-photon router. The operation principle is explained as follows [see Fig. 2(c)].

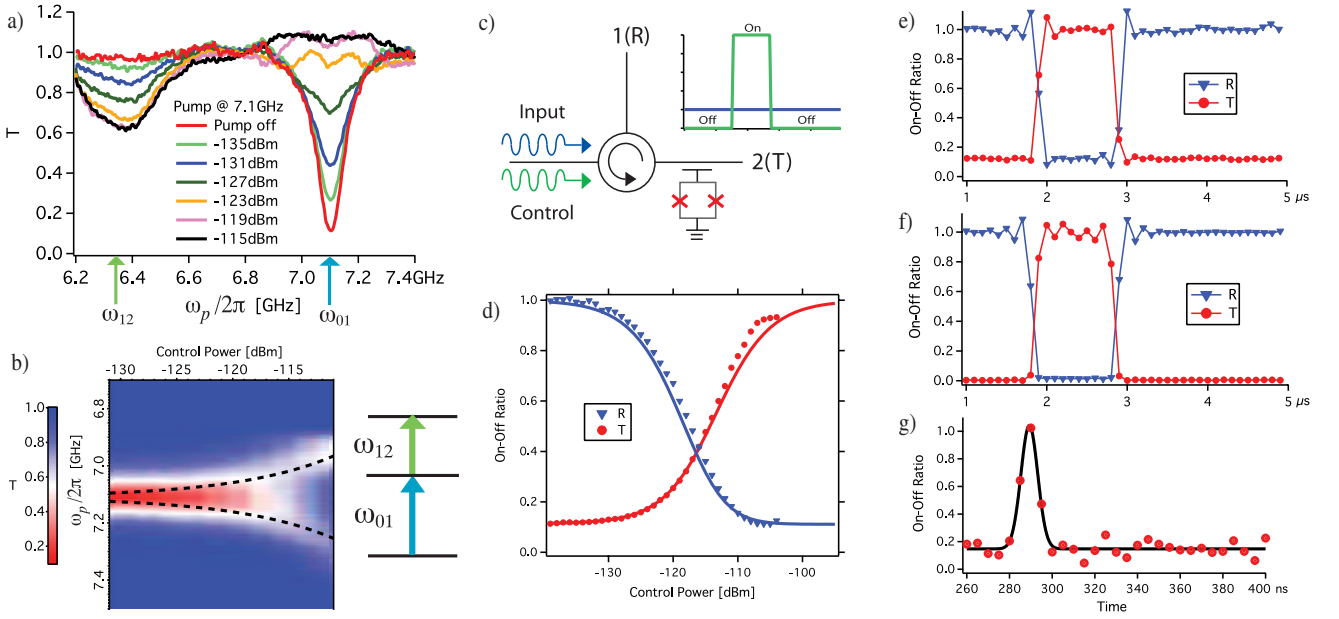

FIG. 2 (color online). (a) Two-tone spectroscopy of sample 1. A microwave pump is continuously applied at ω_{01} with increasing power while a weak probe tone is swept in frequency. As the population in the first state is increased, due to the drive at ω_{01}, scattering at ω_{12} becomes possible, appearing as another dip in the transmittance. From this, we extract $\omega_{12}/2\pi = 6.38$ GHz. (b) The microwave pump is now applied at ω_{12}. As the power of the ω_{12} pump increases, we see electromagnetically induced transparency (EIT) at ω_{01} as the Autler-Townes doublet splits with a separation equal to the Rabi frequency $\Omega_c/2\pi$ (black dashed lines). (inset) Energy level diagram. (c) Cartoon of the router. With the control off, the input probe is reflected from the transmon, and is routed to port 1 through the circulator. When the control is on, the input is transmitted to port 2. Inset: the control pulse sequence. (d) Normalized on-off ratio (see text) of the transmittance (T) and reflectance (R) as a function of control pulse power, measured simultaneously on sample 1. The symbols are the data and the solid lines are fits. (e) Time dependence of T and R at ω_{01}, measured simultaneously for sample 1, while a control pulse is applied. (f) Same for sample 2, although T and R are measured separately. We see that the input signal is routed with an on-off ratio of ~90% (~ 99%) for sample 1 (2). (g) The response of sample 1 to a 10 ns Gaussian control pulse (circles), along with a Gaussian fit (solid line). We see that the transmittance smoothly follows the control on the few ns time scale while maintaining the high on-off ratio.

We input a weak, continuous probe in the single-photon regime at ω_{01}. We then apply a strong control pulse, around 30 dB stronger than the probe, at $\omega_c = \omega_{12}$. When the control is off, the photons are reflected by the atom and travel through the circulator to output 1. When the control is on, the photons are transmitted due to EIT, and travel to output 2. The measurement setup is shown in Fig. 1(b), which enables us to measure the reflected and transmitted probe power simultaneously in the time domain. This is crucial to demonstrate that the extinction of the transmitted beam is due to reflection instead of loss. One could also envision making a photon router by simply detuning the 0–1 transition of the atom via magnetic flux through the SQUID loop. However, the power needed to generate a flux sufficient to detune our atom is several orders of magnitude higher [19].

The operation of the router is demonstrated in Figs. 2(e)–2(g). As expected, when the control is on, most of the signal is transmitted while little is reflected. For sample 2 (1), we achieve an on-off ratio of nearly 99% (90%) in both the reflectance and transmittance. We also characterized the time response of the router. For both devices, we saw no reduction in the on-off ratio down to the shortest pulses, which had a Gaussian full width at half maximum of 10 ns. An example is shown for sample 1 in Fig. 2(g). We see that the transmission follows the control on the few ns time scale, limited by the 5 ns time resolution of our instruments. We would expect the limit of the device to be $\sim 1/\Gamma_{01} = 2$ ns.

In Fig. 2(d), we characterize the on-off ratio as a function of control power for sample 1. We use the experimentally accessible on-off ratio here, because it is not possible to do a full calibration of r (see below). For a probe power in the single-photon regime ($\Omega_p \ll \Gamma_{01}$) with the control and probe on resonance, the transmission of the probe, for a control amplitude corresponding to Ω_c, is [15]

$$t(\Omega_c) = 1 - \frac{\Gamma_{10}}{2\gamma_{10} + \frac{\Omega_c^2}{2\gamma_{20}}}, \tag{3}$$

where γ_{20} is the decoherence rate of the 0–2 transition. Because of the larger dipole moment of the 1–2 transition [16], we have $\Omega_c(P) = \sqrt{2}\,\Omega_p(P)$. We define the *coherent* transmittance and reflectance as $T(\Omega_c) = |t(\Omega_c)|^2$ and

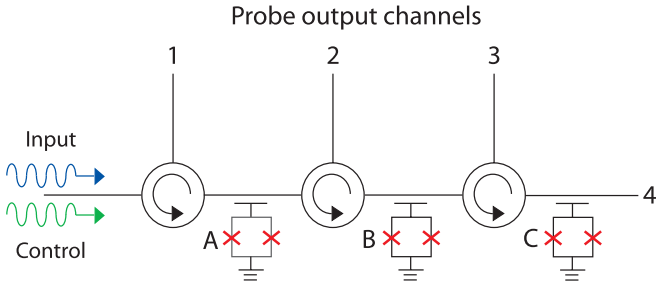

ω_A ω_B ω_C	Off Off Off	On Off Off	On On Off	On On On
Output	1	2	3	4

FIG. 3 (color online). Cartoon of a multiport router. The router demonstrated here can easily be cascaded to distribute photons to many channels. Here we show a four-port router using 3 atoms (A,B,C) in series, each separated by a circulator. The 0–1 transition frequencies of the atoms are the same, while the 1–2 transition frequencies, $\omega_A \neq \omega_B \neq \omega_C$, are different. This arrangement can be designed in a straightforward manner by controlling the ratio of E_J/E_c. By turning on and off control tones at the various 1–2 transition frequencies, we can determine the output channel of the probe field, according to the table. For instance, if we wish to send the probe field to channel 3, we apply two control tones at ω_A and ω_B. We note that all the control tones can be input through the same port regardless of the number of output channels, reducing the complexity of the design.

$R(\Omega_c) = |1 - t(\Omega_c)|^2$, respectively. An important point is that not all of the input power is necessarily transmitted and reflected coherently. For intermediate values of Ω_c, a significant fraction of the power, quantified by $1 - R(\Omega_c) - T(\Omega_c)$, is lost to spontaneous emission at various frequencies. This power is not detected by our phase-sensitive voltage measurement. To fit the reflection data, we use the theoretical on-off ratio $[R(\Omega_c) + R_b]/[R(0) + R_b]$, where R_b accounts for background reflections in the line and leakage through circulator 2 [Fig. 1(b)]. Using the same values of Γ_{10} and γ_{10} as before, we extract the additional parameters $\gamma_{20}/2\pi = 145$ MHz and $R_b = 0.05$. These values agree with our expectations based on the charge dispersion of $|2\rangle$ and circulator leakage in our system.

It is natural to ask, why sample 2 outperforms sample 1. Within the current model, the switching efficiency η is limited by the maximum reflectance $R_{\max} = (\Gamma_{10}/2\gamma_{10})^2 \approx 1–4\Gamma_\varphi/\Gamma_{10}$, which is limited by pure dephasing. The major improvement therefore comes from the reduction of the pure dephasing from 18 MHz to 2 MHz. This reduction can largely be attributed to the increase of E_J/E_c from 22 to 60, which dramatically reduces the sensitivity of the transmon to charge noise [16]. A smaller effect is the increased coupling, with $\Gamma_{10}/2\pi$ changing from 73 to 96 MHz.

The operation scheme of the router is scalable in a straightforward manner, as is explained in detail in Fig. 3. For an n-port router, the routing efficiency to the kth port is $\eta_k = T^{k-1}R$ for $k \neq n$ and $\eta_n = T^{n-1}$ for $k = n$. For sample 2, we measure $T \approx 99\%$ and $R \approx 92\%$. Therefore, the efficiency of a four-port router would still exceed 90%. This could be further improved by further reducing the dephasing.

In conclusion, we have demonstrated a basic single-photon router with high speed and efficiency operating in the microwave regime. While microwave circuits are a promising technology for quantum nodes, it is clear that optical photons are advantageous for use in quantum channels. This identifies the development of an optical-microwave quantum interface as a key enabling technology for a hybrid quantum network. Early steps to this type of interface have recently been achieved by a number of groups [32,33].

We acknowledge financial support from the Swedish Research Council, the Wallenberg foundation and from the EU through the European Research Council and the integrated project SOLID. B. P. acknowledges CSIC JAE-PREDOC2009, FIS2009-10061, and QUITEMAD S2009-ESP-1594. We would also like to acknowledge O. Astafiev for fruitful discussions and M. Sandberg and F. Persson for fabrication and experimental help.

[1] V. Scarani *et al.*, Rev. Mod. Phys. **81**, 1301 (2009).
[2] H. J. Kimble, Nature (London) **453**, 1023 (2008).
[3] D. A. Braje *et al.*, Phys. Rev. A **68**, 041801 (2003).
[4] S. E. Harris and L. V. Hau, Phys. Rev. Lett. **82**, 4611 (1999).
[5] S. E. Harris and Y. Yamamoto, Phys. Rev. Lett. **81**, 3611 (1998).
[6] J. T. Shen and S. H. Fan, Opt. Lett. **30**, 2001 (2005).
[7] J. T. Shen and S. H. Fan, Phys. Rev. Lett. **95**, 213001 (2005).
[8] G. Zumofen *et al.*, Phys. Rev. Lett. **101**, 180404 (2008).
[9] D. Witthaut and A. S. Sorensen, New J. Phys. **12**, 043052 (2010).
[10] M. K. Tey *et al.*, Nature Phys. **4**, 924 (2008).
[11] J. Hwang *et al.*, Nature (London) **460**, 76 (2009).
[12] G. Wrigge *et al.*, Nature Phys. **4**, 60 (2007).
[13] I. Gerhardt *et al.*, Phys. Rev. Lett. **98**, 033601 (2007).
[14] O. Astafiev *et al.*, Science **327**, 840 (2010).
[15] A. A. Abdumalikov *et al.*, Phys. Rev. Lett. **104**, 193601 (2010).
[16] J. Koch *et al.*, Phys. Rev. A **76**, 042319 (2007).
[17] D. I. Schuster *et al.*, Nature (London) **445**, 515 (2007).
[18] J. M. Fink *et al.*, Nature (London) **454**, 315 (2008).
[19] M. Sandberg *et al.*, Phys. Scr. **T137**, 014018 (2009).
[20] F. Mallet *et al.*, Nature Phys. **5**, 791 (2009).
[21] L. DiCarlo *et al.*, Nature (London) **460**, 240 (2009).
[22] A. A. Houck *et al.*, Nature (London) **449**, 328 (2007).
[23] D. E. Chang *et al.*, Nature Phys. **3**, 807 (2007).
[24] See Supplemental Material at http://link.aps.org/supplemental/10.1103/PhysRevLett.107.073601 for measurements and fitting of the transmission coefficient.
[25] M. Baur *et al.*, Phys. Rev. Lett. **102**, 243602 (2009).

[26] B. R. Mollow, Phys. Rev. **188**, 1969 (1969).
[27] M. Fleischhauer *et al.*, Rev. Mod. Phys. **77**, 633 (2005).
[28] W. R. Kelly *et al.*, Phys. Rev. Lett. **104**, 163601 (2010).
[29] L. Slodička *et al.*, Phys. Rev. Lett. **105**, 153604 (2010).
[30] S. H. Autler and C. H. Townes, Phys. Rev. **100**, 703 (1955).
[31] P. M. Anisimov *et al.*, arXiv:1102.0546v1.
[32] Y. Kubo *et al.*, Phys. Rev. Lett. **105**, 140502 (2010).
[33] D. Schuster *et al.*, Phys. Rev. Lett. **105**, 140501 (2010).